SANDIA REPORT
SAND201X-XXXX
Unlimited Release
Printed September 2019

Cooperative self-assembly for structure and morphology control of energetic materials

Hongyou Fan, David Rosenberg, Leanne Alarid, Kaifu Bian, Casey Karler, Hattie Schunk, Brian Billstrand, Erick Ortiz

Prepared by
Sandia National Laboratories
Albuquerque, New Mexico 87185 and Livermore, California 94550

Sandia National Laboratories is a multimission laboratory managed and operated by National Technology and Engineering Solutions of Sandia, LLC, a wholly owned subsidiary of Honeywell International, Inc., for the U.S. Department of Energy's National Nuclear Security Administration under contract DE-NA0003525.

Issued by Sandia National Laboratories, operated for the United States Department of Energy by National Technology and Engineering Solutions of Sandia, LLC.

Available to DOE and DOE contractors from
U.S. Department of Energy
Office of Scientific and Technical Information
P.O. Box 62
Oak Ridge, TN 37831

Telephone: (865) 576-8401
Facsimile: (865) 576-5728
E-Mail: reports@osti.gov
Online ordering: http://www.osti.gov/scitech

Available to the public from
U.S. Department of Commerce
National Technical Information Service
5301 Shawnee Rd
Alexandria, VA 22312

Telephone: (800) 553-6847
Facsimile: (703) 605-6900
E-Mail: orders@ntis.gov
Online order: https://classic.ntis.gov/help/order-methods/

SAND201X-XXXX
Printed September 2018
Unlimited Release

Cooperative Self-Assembly for Structure and Morphology Control of Energetic Materials

Hongyou Fan, David Rosenberg, Leanne Alarid, Kaifu Bian, Casey Karler, Hattie Schunk, Brian Billstrand, Erick Ortiz

Department Name(s)
Sandia National Laboratories
P. O. Box 5800
Albuquerque, New Mexico 87185-MS1349

Abstract

The performance of energetic materials (EM) varies significantly across production lots due to the inability of current production methods to yield consistent morphology and size. Lot-to-lot variations and the inability to remake the needed characteristics that meet specification is costly, increases uncertainty, and creates additional risk in programs using these materials. There is thus a pressing need to more reliably formulate EMs with greater control of morphology. The goal of this project is to use the surfactant-assisted self-assembly to generate EM particles with well-defined size and external morphologies using triaminotrinitrobenzene (TATB) and hexanitrohexaazaisowurtzitane (CL-20) as these EMs are both prevalent in the stockpile and present interesting/urgent reprocessing challenges. We intend to understand fundamental science on how molecular packing influences EM morphology. We develop scale up fabrication of EM particles with controlled morphology, promising to eliminate inconsistent performance by providing a trusted and reproducible method to improve EMs for NW applications.

ACKNOWLEDGMENTS

The authors wish to acknowledge the work of Marley Apperson, Amy Allen, Barry Ritchie, Laura Martin, Kathy Alam, Ryan Marinis, and Duane Richardson for their contributions to the effort to scale-up CL-20 to the 1g level and it's characterization.

TABLE OF CONTENTS

FIGURES

NOMENCLATURE

Abbreviation	Definition
EM	energetic materials
CL20	hexanitrohexaazaisowurtzitane
TATB	triaminotrinitrobenzene or 2,4,6-triamino-1,3,5- trinitrobenzene
EtOAc	Ethyl acetate
OCT	octane

1. BACKGROUND

The morphology of EM crystalline particles is governed by well-understood intermolecular interactions such as Van der Waals forces, dipole interactions, etc. Techniques used to influence or control particle morphology have been essentially unchanged for centuries: precipitation, re-crystallization, and physical manipulation (grinding). The final products obtained using these technologies exhibit irregular morphology and size as well as varying degrees of particle size distribution. Recent advances in material processing, typically appropriated from pharmaceutical applications, have provided some incremental improvements in control of EM morphology: spray-drying, lyophilization, use of ionic-liquid or super-critical solvent systems, etc. Unfortunately, these new technologies, when successful, only reduce already existing variability and fail to provide the desired level of morphological control.

Surfactant assisted molecular self-assembly is a powerful method to fabricate hierarchical organic crystal nanostructures with well-defined shapes that impart multifunctionality derived from individual starting molecules or molecular building blocks.[1-8] Amphiphilic molecules (or surfactants) with hydrophilic head groups and hydrophobic tail groups form micelles with hydrophobic compartments. Through encapsulation, hydrophobic species (molecules, oil, etc.) can be introduced into the hydrophobic interior and initiate confined self-assembly of organic crystals. Based on this generic phenomenon, Sandia has pioneered the development of the cooperative self-assembly method by combining non-covalent interactions, such as van der Waals, hydrogen bonding, etc., between functional building blocks (e.g., optically active porphyrins)[9] and amphiphilic surfactants to direct or confine nucleation and growth of well-defined crystalline nanostructures within surfactant micelles. In recent work, we showed that protonation/de-protonation or solubility based phase transition facilitates the confined cooperative self-assembly process for fine-tuning of 1-3D active particles with controlled external morphology and function at multiple length scales and positions (Fig 1). [1-8, 10]

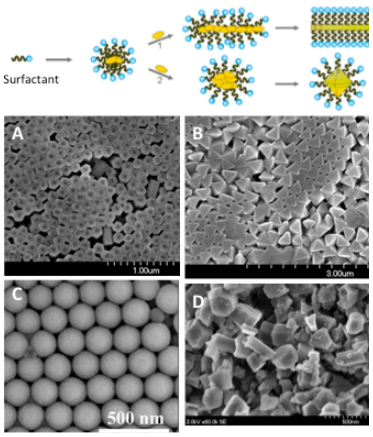

Fig. 1 Morphology control of self-assembled nanostructures using organic compound zinc meso-tetra (4-pyridyl) porphyrin as the building block through micelle confined protonation and solvation.

Cartoon shows surfactant micelle confined growth and formation of controlled morphology. (A,B,C) SEM images of monodisperse particles with well-defined shape. D shows irregular morphology without using surfactants.

We extended this method to reprocess EMs to have well-defined external morphologies using triamino-trinitro-benzene (TATB) and hexanitrohexaazaisowurtzitane (CL-20) as these EMs are both prevalent in the stockpile and present interesting reprocessing challenges. The idea is to sequester the EMs within surfactant micelles in solutions through either protonation/de-protonation or solubility based phase transition. Using this self-assembly process, we investigated the fundamental science of morphology control during self-assembly. We performed advanced in-situ characterizations using x-ray scattering, electron microscopy, and spectroscopy to characterize the final EM particles.

2. EXPERIMENTS AND CHARACTERIZATIONS

2.1. CL-20 Recrystallization

2.1.1. 10mg scale

To produce CL-20 particles, CL-20 powder was first dissolved in ethyl acetate (EtOAc) and stirred mildly until complete dissolution to obtain 5 mg/mL clear solution.[11] Separately, a surfactant solution of Span80 (10 mM) was prepared in octane (OCT). Then 1.0 mL of CL-20 solution was added into 10 mL of Span80/OCT solution and shaken to mix. Neither visible precipitation nor phase separation occurred. While stirring, vacuum of 8 torr was applied to the mixture to preferentially remove EtOAc which has a lower boiling point than OCT. After approximately 14 minutes, the solution became slightly cloudy with fine white precipitates visible. The cloudiness increased and was more fully noticeable at 17 minutes. It was allowed to stir for 2 hours for complete reaction. The final suspension appeared very cloudy with fine white precipitate which was washed twice with hexane to remove any residual surfactant remaining in the solution and the solid product was re-dispersed in 1mL hexane for storage.

2.1.2. 1g scale

To obtain sufficient material to perform functional evaluation the experimental procedure detailed above (carried out at the 5 mg scale) was scaled-up to the 1g level. Scale up provided several challenges, the two main hurdles being the extreme dilution required for the process to succeed, and the time scale for solvent removal (both of which were determined to be critical for success). The development scale uses 1ml of a 5mg/ml solution of CL-20 in EtOAc, diluted into 10ml of the non-solvent as a starting point and removes the 1ml of solvent under reduced pressure over approximately 20 minutes. After attempting more concentrated conditions to reduce volume, success was initially achieved at the 0.25 g scale using the same ratio of CL-20 to solvent and a 1:5 solvent to non-solvent ratio (rather than 1:10). Normal agitation was not sufficient to remove the solvent from this mixture in less than an hour, a rotary evaporator was used and a heating bath was required to maintain the solution at ambient temperature over the course of the evaporation. Product from this process was centrifuged and washed with hexane to remove residual solvent and surfactant.

2.2. Preparation of TATB particles

To produce TATB microparticles, 10 mg TATB powder was first dissolved in 400 µL 1-butyl-3-methylimidazolium acetate (BMA) ionic liquid by heating the mixture to 110 °C for about 15 mins. In a 20 mL glass vial, span 80 surfactant was added into 10 mL octane to obtain 10 mM solution. 100 µL TATB-BMA solution was injected in to the span 80 solution while being sonicated using a Qsonica Q125 sonicator operated at 60% power. An opaque and milky solution was obtained instantly, indicative of micelle formation. To precipitate TATB and form microparticles, with continuous sonication, 5 mL of anti-solvent (water or ethanol) was added dropwise to reduce solubility of TATB in the micelles. The mixture slowly turned cloudy and yellow precipitation of TATB was visually apparent. The raw product was separated by centrifugation to isolate the yellow precipitate which was then washed with hexane and ethanol to remove any residual solvent, surfactants, or BMA. The final product was dispersed in a small amount of ethanol for storage and characterizations. The resulting slurry was drop-cast onto silica

wafers, dried in atmosphere, and repeated as necessary to achieve sufficient film thickness for characterization.

2.3. Characterization Methods

SEM characterization was performed on a Hitachi S-5200 Scanning Electron Microscope operating at 2.0kV and 15 μA. SEM samples were prepared by drop-casting CL-20 particles suspended in hexane onto a silicon wafer. Particle size information was obtained by manually counting 200 particles in SEM images. Raman spectroscopy was performed on a Thermo Scientific DXR Smart Raman instrument with 780 nm laser. Powder X-ray diffraction (PXRD) was performed using a PANalytical X'Pert PRO operating at 45 kv and 40 mA. Both Raman and PXRD samples were prepared by drop-casting onto thin glass slides.

3. RESULTS AND DISCUSSION:

3.1. Development of CL-20 process

3.1.1. mg scale

As illustrated by Fig. 2 CL-20 was first dissolved in a good solvent (EtOAc) which was then added into an anti-solvent (OCT) of the opposite polarity along with Span 80 as surfactant. Span 80 was chosen because it facilitates the self-assembly of water-in-oil type micelles encapsulating the good solvent.[11] Then EtOAc, with a higher vapor pressure, was preferentially removed by vacuum-induced evaporation to precipitate the solute and form CL-20 particles. Vacuum allows solvent removal at room temperature. The particle size and uniformity were strongly defined by the concentration of target materials as well as size and quality of micelles.

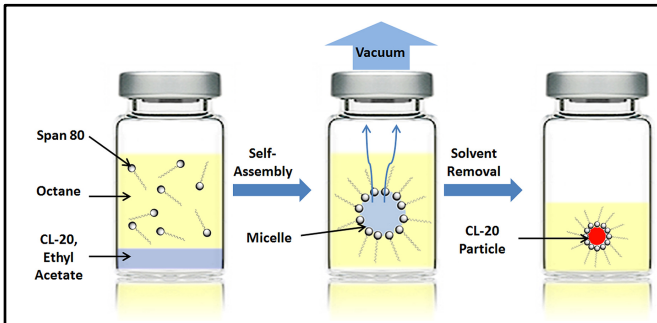

Fig. 2 Schematic illustration of the surfactant assisted self-assembly and crystallization of CL-20 particles under vacuum.

A representative SEM image of the product CL-20 particles is shown in Fig. 3a. Using the micelle based methods, nearly spherical particles were obtained. the particles of highest quality displayed a small average diameter of 985 nm with a very narrow size distribution evidenced by a standard deviation of 138 nm, or 14%. This is a significant improvement in microscopic morphology, compared with the as-received raw material of CL-20 powder which contains faceted particles of several microns and shows no sign of monodispersity in either size or shape (Fig. 3b).

Under ambient conditions, CL-20 may exist as one of four polymorphic phases namely α, β, γ, and ε.[12, 13] It is desirable to obtain pure-phase CL-20 particles even though most of the recrystallization led to mixture of different crystal structures.[5] To confirm the composition, these spherical microparticles were characterized by XRD and Raman Spectroscopy. The XRD pattern in Fig. 4 revealed that the CL-20 particles have an orthorhombic β-phase crystal structure. All of the peaks were indexed to belong to an orthorhombic lattice with lattice parameters a = 9.684 Å, b = 11.587 Å and c = 12.987 Å. It is consistent with literature values[14] with very slight volumetric lattice shrinkage of 0.5% which can possibly be explained by inward surface tension due to small particle size. As another feature we observed in the XRD pattern, (002) was stronger than (111) peak. However in an ideal powder sample of orthorhombic crystal, (002) peak is predicted to be approximately four times weaker than (111) peak. The exceptionally strong (002) peak in our case indicates better stacking ordering in the c-axis. It also suggests Span 80 interfered with crystal growth in a and b directions and prevented the formation of larger faceted particles.

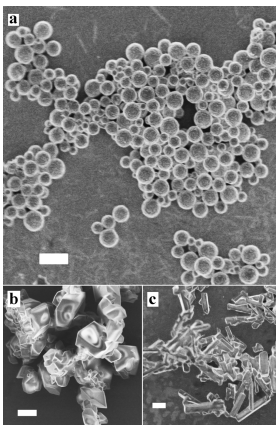

Fig. 3 SEM images of CL-20 particles.

(a) CL-20 particles crystalized using the surfactant assisted self-assembly and crystallization. (b) Raw CL-20 feedstock powders. (c) CL-20 particles from controlled crystallization without using surfactants. The scale bars are 2 μm.

We also monitored this microparticle formation in a static heterogeneous experiment using in-situ dynamic light scattering (DLS) measurement.[15] As an efficient optical method, DLS provided a quick statistical analysis on particle size in a suspension. Therefore DLS is ideal to trace the growth of CL-20 microparticles without interrupting it. However, the theory and method of DLS measurements forbid external perturbation to the system such as stirring. Consequently we had to perform an indirect exploration of the process where a heterogeneous growth in static liquid was tracked by DLS. To extract critical parameters such as CL-20 solubility in the binary solvent mixture, the time-resolved DLS results were interpreted by a finite element model to simulate the microparticle formation and migration in the heterogeneous system. These parameters were then used to predict the particle growth behavior and product quality of homogenous batch synthesis.

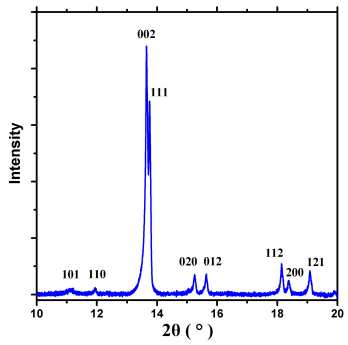

Fig. 4 XRD pattern of the CL-20 particles synthesized by the micelle confinement method reveals the orthorhombic β-phase of molecular crystal lattice.

The peaks are labeled with corresponding Miller indices.

3.1.2. gram scale

A number of conditions were explored during the effort to scale up the above process to the 1g+ scale. A specific effort to optimize the process was not made, the scope of the work was limited to a feasibility study to demonstrate that the results obtained at the very small scale above could be repeated on a larger scale. However, given equipment and facility constraints, initial efforts explored the possibility of obtaining similar results in a more concentrated environment (1:1 solvent to non-solvent ratio while conserving the surfactant ratio in non-solvent). While the results were striking (Figure 5), and may bear further characterization and exploration, they did not replicate the smaller scale material. In addition, early efforts to scale up maintained the stir

agitation used at the small scale, but this became untenable as volumes increased and time to complete removal of EtOAc became extended (unheated stripping with stirring resulted in more than 9 hours required to produce solid). Using a Rotovap to effect the solvent stripping, using a heated water bath to maintain the solvent reservoir at ambient temperature, initially resulted in solvent removal (and precipitation of solid) in 22 minutes. However, the solid recovered from this procedure consisted of imperfect, partially formed spheres; while particles had spherical overall shape, they were riddled with voids and were not typical of the small scale results (Figure 6a). Controlling the vacuum to double the time required for solvent removal resulted in solid appearing particulates with very low particle size distribution (Figure 6b). Upon scaling this to 1g level, the increase in solvent volume necessitated switching from a 1L solvent reservoir to a 5L reservoir. This resulted in significantly changed mixing dynamics which manifested as changes in product morphology. Subsequent developmental procedures showed that both the time required for solvent stripping, and flask rotational speed had effects on product morphology; longer stripping times produced more perfected, but larger spherical particles (figure 7a). Finally, the 1g process that produced the closest analog to the material obtained in the mg scale effort required changing the vacuum pump used to one with a higher throughput to allow for faster solvent stripping at the liter scale. This procedure used 1g of CL-20 in 200ml EtOAc, combined with 1L octane in a 5L reservoir. The EtOAc was stripped off under the maximum vacuum available to the pump used while maintaining the reservoir at ambient temperature and rotating at a speed that produced approximately the same centrifugal force at the reservoir wall as was found in the 0.25g scale process (which used a 1L reservoir). This produced spherical material with size scale larger than desired (figure 7b) and exhibiting larger particle size distribution than even the 0.25g results, but yielded enough material for functional evaluation (which was the goal). The powders shown in figure 7 were characterized using RAMAN IR to determine polymorph. Results of this analysis showed both samples to be mainly β with a small (<5%) contaminant of ε. The material was not

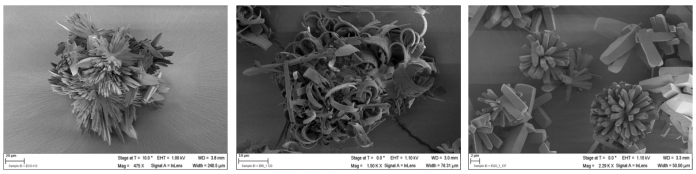

Fig. 5 SEM images of CL-20 crystals resulting from initial scale up efforts.

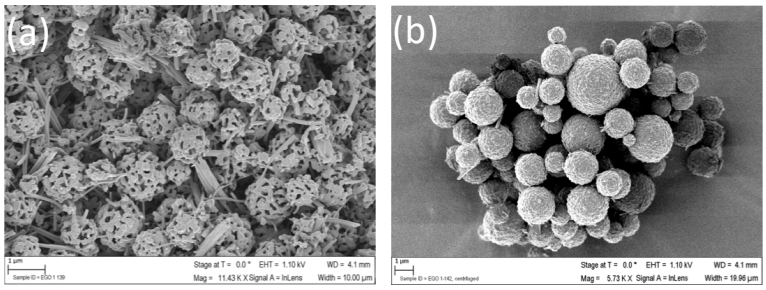

Fig. 6 SEM images of CL-20 particles.

a) 0.25 g scale, 150 rpm, 15 torr , 22 mins. b) 0.25 g scale, 150 rpm, 22 torr, 44 mins.

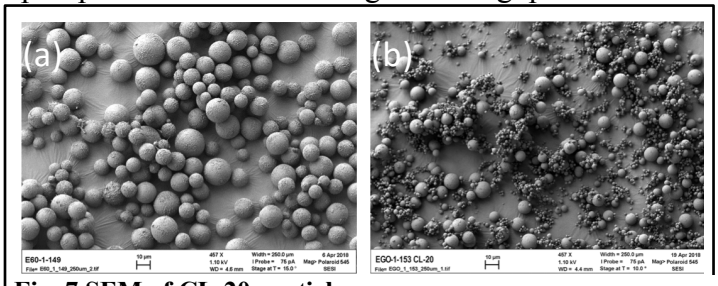

Fig. 7 SEM of CL-20 particles.

a) 1g scale, 120 rpm, 53 torr, 47 mins. b) 1 g scale, 114 rpm, 22 torr, 39 mins

subjected to liquid chromatography to characterize CL-20 purity or residual surfactant due to the concern that surfactant could catastrophically contaminate the UPLC instrument.

While there was no expectation that this method would produce usable material without additional development or optimization, the produced powder was subjected to a cursory functional evaluation in an exploding bridgewire (EBW) device. The CL-20 powder shown in figure 7 was loaded into a standard header at ~50% TMD and subjected to a 1500V firing signal (detonator grade CL-20 exhibits a threshold of 350-550V in the same configuration and fire-set). Neither material transitioned to detonation under the conditions though all loaded powders deflagrated. This result was not surprising given the optimization that is required to produce detonator grade CL-20.

3.2. Development of TATB process

The TATB microparticle growth in this study was modified from a micelle-confinement method which was previously developed to synthesize a variety of molecular crystalline particles. Briefly, as demonstrated by Fig. 8, TATB was first dissolved in BMA ionic liquid. Ionic liquid was chosen as the carrier solvent to achieve practical TATB solubility, high polarity contrast against octane in moderate operation conditions. TATB/BMA was then added in an octane solution of surfactant Span 80. The mixture was then sonicated to form micelles encapsulating TATB/BMA. In earlier studies for particle synthesis of other materials, particle formation was triggered by evaporating the carrier solvents by either heat or vacuum. However in this work, due to the high boiling point of ionic liquid, TATB particle precipitation within micelles was achieved by adding water as an anti-solvent precipitant into the system. Water was strongly attracted into micelles by the ionic liquid and drove the oversaturation and rapid precipitation of TATB which is insoluble in water. The mixture quickly became a homogenously cloudy suspension particle formation. Finally the product TATB precipitates were collected and cleaned by centrifugation.

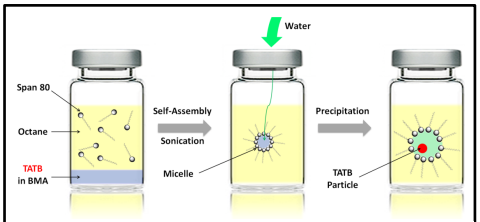

Fig. 8 Schematic growth process of TATB microparticles.

Optical microscopy (Fig 9a) of the product revealed uniform TATB microparticles in yellow color. At higher resolution, the SEM image of Fig. 9b confirmed a quasi-spherical morphology of the TATB microparticles. Statistically these particles averaged a diameter of 1.48 μm with standard deviation of only 0.14 μm (9.5%), meaning a dramatic improvement of monodispersity over the raw TATB powder (Fig. 9c) which contained particles of tens of microns with broad size distribution. These quasi-spherical microparticles are by far the most uniform TATB particles to the best of our knowledge. They would potentially improve performance and reproducibility of explosive devices.

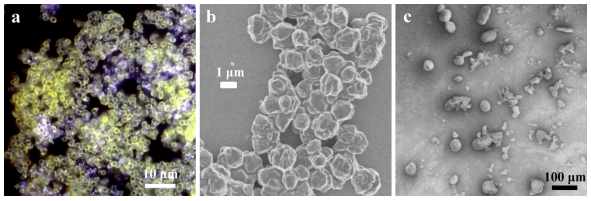

Fig. 9 Images of TATB microparticles.

(a) Optical micrograph of the yellow particles produced by the micelle-confinement method. The purple areas are artifacts caused by lens chromatic aberration. SEM images of (b) TATB microparticles and (c) as-received TATB powder.

To confirm the composition of the product microparticles, they were examined by XRD measurements. The red signal in Fig. 10 presents the XRD pattern of the microparticles. By

comparing it with that from raw material TATB, it was found that the microparticles are in good agreement with the triclinic TATB crystal structure (space group P-1) with lattice parameters of a = 9.01, b = 9.03, c = 6.81 Å and α = 108.6°, β = 91.8°, γ = 120.0°. In such lattice, the hexagonal disk-like TATB molecules formed robust monolayers as the a-b plane via strong hydrogen bonds between their nitro and amine groups. The monolayers then piled up in c direction forming the triclinic lattice. It is worth noting that the diffraction peaks from the microparticles displayed noticeably weakened and broadened peaks with respect to the ;bulk materials. This is a result of reduced crystalline size and lattice ordering, consistent with the micron-sized quasi-spherical particle shape with little faceted features.

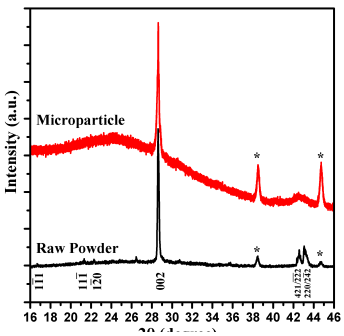

Fig. 10 XRD patterns of TATB raw powder (black) and microparticles (red).

The peaks were identified and labeled with their Miller indices.

The significantly improved morphology and uniformity are attributed to the surfactant-driven micelle formation. To study the mechanism, a control experiment was conducted under the same conditions except for the absence of surfactants. In this case, large chunks of yellow agglomerates were produced upon addition of water. According to SEM image (Fig. 11a) the agglomerates showed a branched and sponge-like morphology. Interestingly the sponge structure possessed nanoscale texture that is believed to be caused by the strong shear forces induced by sonication during the recrystallization of TATB. The increased surface area/volume ratio of the sponge TATB could potentially provide improved discharge performance while its high porosity might limit EM energy density. Such significant morphological differences provide strong evidence that the presence of surfactants is crucial to the synthesis of the quasi-spherical TATB microparticles.

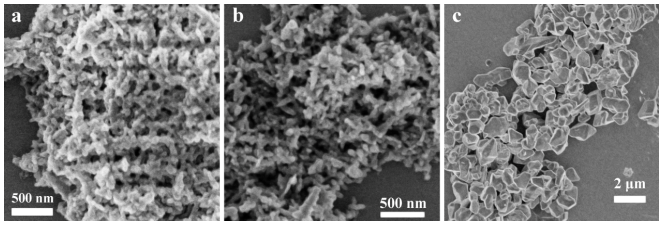

Fig. 11 SEM images of TATB products from control experiments.

(a) Without surfactants, (b) using SDS surfactant and (c) using Span 80 surfactant but ethanol as the precipitant.

To obtain deeper insights into the role of the Span 80 surfactant (an inexpensive surfactant widely used in food and cosmetic industries) and confirm the micelle confinement mechanism, the process was repeated with another common ionic surfactant sodium dodecyl sulfate (SDS). As an effective indicator, the hydrophilic-lipophilic balance or HLB is a parameter widely used to evaluate and predict the performance of surfactants. Surfactants with HLB ranging between 3 and 8 are ideal emulsifiers for water-in-oil type micelles. Span 80 has a HLB of 4.3 and was predicted to encapsulate the highly polar ionic liquid in the continuous non-polar phase of octane. On the other hand, SDS with a much higher HLB value of 40 is favorable for oil-in-water type emulsion and was not expected to form micelles in this work. The product shown by Fig. 11b displayed very similar TATB morphology to the no-surfactant case, suggesting that the reason that SDS does not lead to microparticles is due to lack of micelle formation in the given solvent system. This result further confirmed the important role of a carefully chosen surfactant with a proper HLB in terms of reliable micelle formation.

As an effort to study the relationship between recrystallization speed and the morphology of the TATB microparticles, water was replaced by ethanol as precipitant. Ethanol is miscible with

both BMA and octane. Therefore with the same injection rate, less precipitant would enter the BMA micelles causing a slower recrystallization process of TATB. As shown by Fig. 11c, ethanol resulted in TATB particles of similar micron size but faceted morphology. On one hand, slower recrystallization provided longer relaxation time for the formation of crystalline solid with better ordering and lower free energy. On the other hand, the rapid recrystallization with water increased the likelihood of incorporating impurities such as surfactants into TATB particles and reduced the tendency to form faceted features.

4. CONCLUSIONS

We developed and scaled up to 1g level a surfactant assisted self-assembly method to crystalize spherical CL-20 microparticles. Several process factors are critical for the formation of uniform spherical morphology including using low boiling solvents such ethyl acetate, type of surfactants and concentration, processing temperature, pressure, and agitation. The average particle size centered at approximately 1 μm for 5mg scale and 5μm for 1g scale. XRD results detect orthorhombic β-phase crystal structure at the 5mg scale. This polymorph was confirmed at the 1g scale using Raman IR. The uniform spherical morphology of these particles demonstrates a significant improvement in microstructure control compared with other crystallization methods. An inexpensive and rapid synthesis of monodispersed TATB microparticles was developed based on recrystallization of TATB within surfactant micelles in ionic liquid. The choice of a surfactant with proper hydrophilic-lipophilic balance value was the key to micelle formation and therefore successful microparticle production. Depending on recrystallization speed of TATB, different microparticle morphologies of either quasi-spherical or faceted were obtained. This level of morphological control represents a completely new capability in energetic material processing, one whose ramifications have not even begun to be explored. This method of particle production presents a potentially powerful new tool for EM morphology control with possible applications in both modeling definition/validation and achieving tailored material functional behavior.

REFERENCES

1. Bai, F.; Sun, Z.; Wu, H.; Haddad, R. E.; Coker, E. N.; Huang, J. Y.; Rodriguez, M. A.; Fan, H. Porous One-Dimensional Nanostructures through Confined Cooperative Self-Assembly. *Nano Letters* **2011**, *11*, 5196-5200.
2. Bai, F.; Sun, Z.; Wu, H.; Haddad, R. E.; Xiao, X.; Fan, H. Templated Photocatalytic Synthesis of Well-Defined Platinum Hollow Nanostructures with Enhanced Catalytic Performance for Methanol Oxidation. *Nano Letters* **2011**, *11*, 3759-3762.
3. Wang, D.; Niu, L.; Qiao, Z.-Y.; Cheng, D.-B.; Wang, J.; Zhong, Y.; Bai, F.; Wang, H.; Fan, H. Synthesis of Self-Assembled Porphyrin Nanoparticle Photosensitizers. *ACS Nano* **2018**, *12*, 3796-3803.
4. Wang, J.; Zhong, Y.; Wang, X.; Yang, W.; Bai, F.; Zhang, B.; Alarid, L.; Bian, K.; Fan, H. pH-Dependent Assembly of Porphyrin–Silica Nanocomposites and Their Application in Targeted Photodynamic Therapy. *Nano Letters* **2017**, *17*, 6916-6921.
5. Xu, J.; Tian, Y.; Liu, Y.; Zhang, H.; Shu, Y.; Sun, J. Polymorphism in hexanitrohexaazaisowurtzitane crystallized from solution. *J. Crst. Growth* **2012**, *354*, 13.
6. Zhang, N.; Wang, L.; Wang, H.; Cao, R.; Wang, J.; Bai, F.; Fan, H. Self-Assembled One-Dimensional Porphyrin Nanostructures with Enhanced Photocatalytic Hydrogen Generation. *Nano Letters* **2018**, *18*, 560-566.
7. Zhong, Y.; Wang, J.; Zhang, R.; Wei, W.; Wang, H.; Lü, X.; Bai, F.; Wu, H.; Haddad, R.; Fan, H. Morphology-Controlled Self-Assembly and Synthesis of Photocatalytic Nanocrystals. *Nano Letters* **2014**, *14*, 7175-7179.
8. Zhong, Y.; Wang, Z.; Zhang, R.; Bai, F.; Wu, H.; Haddad, R.; Fan, H. Interfacial Self-Assembly Driven Formation of Hierarchically Structured Nanocrystals with Photocatalytic Activity. *ACS Nano* **2014**, *8*, 827-833.
9. Bian, K.; Alarid, L.; Karler, C.; Hwang, A.; Ye, D.; Fan, H. Surfactant-Assisted Synthesis of Tetragonal Porphyrin Microparticles. *MRS Advances* **2018**, 1-6.
10. Billstrand, B.; Bian, K.; Karler, C.; Fan, H. Functionalized Block-Copolymer Templates for Synthesis and Shape Control of Quantum Dots. *MRS Advances* **2018**, *3*, 2429-2433.
11. Bian, K., Alarid, L., Rosenberg, D., & Fan, H. Surfactant Assisted Self-assembly and Synthesis of Highly Uniform Spherical CL-20 Microparticles. *MRS Advances* **2018**, *3*, 2421-2427.
12. Goede, P.; Latypov, N. V.; Ostmark, H. Fourier Transform Raman Spectroscopy of the Four Crystallographic Phases of α, β, γ and ε 2,4,6,8,10,12-Hexanitro-2,4,6,8,10,12-hexaazatetracyclo[5.5.0.05,9.03,11]dodecane (HNIW, CL-20). *Propellants, Explos., and Pyrotech.* **2004**, *29*, 205.
13. Russell, T. P.; Miller, P. J.; Piermarini, G. J.; Block, S. Pressure/temperature phase diagram of hexanitrohexaazaisowurtzitane. *J. Phys. Chem.* **1993**, *97*, 1993.
14. Tan, J.-J.; Ji, G.-F.; Chen, X.-R.; Li, Z. Structure, equation of state and elasticity of crystalline HNIW by molecular dynamics simulations. *Physica B: Condensed Matter* **2011**, *406*, 2925.
15. Bian, K.; Alarid, L.; Rosenberg, D.; Fan, H. Exploration of Processing Parameters of Vacuum Assisted Micelle Confinement Synthesis of Spherical CL-20 Microparticles. *MRS Advances* **2018**, *3*, 553-561.

DISTRIBUTION

4 Lawrence Livermore National Laboratory
Attn: N. Dunipace (1)
P.O. Box 808, MS L-795
Livermore, CA 94551-0808

1	MS1349	Hongyou Fan	1815
1	MS1455	David Rosenberg	2555
1	MS1415	Carlos Gutierrez	1874
1	MS1349	Randy Schunk	1815
1	MS0899	Technical Library	9536 (electronic copy)

For LDRD reports, add:

1	MS0359	D. Chavez, LDRD Office	1911

For CRADA reports add:

1	MS0115	OFA/NFE Agreements	10012

For Patent Caution reports, add:

1	MS0161	Legal Technology Transfer Center	11500


Sandia National Laboratories